# Lattice vibrations of para-hydrogen impurities in a solid deuterium matrix: An inelastic neutron scattering study

D. Colognesi,[1] M. Celli,[1] A. J. Ramirez-Cuesta,[2] and M. Zoppi[1]
[1]*Consiglio Nazionale delle Ricerche, Istituto dei Sistemi Complessi, Sezione di Firenze, via Madonna del Piano 10, Sesto Fiorentino, 50019 Firenze, Italy*
[2]*ISIS Facility, Rutherford Appleton Laboratory, Chilton, Didcot, Oxon OX11 0QX, United Kingdom*
(Received 29 January 2007; revised manuscript received 3 April 2007; published 20 November 2007)

In the present study, we report inelastic neutron scattering measurements from para-hydrogen defects in solid normal deuterium at three different concentrations (between 3% and 11%) using the time-of-flight spectrometer TOSCA-II. The measured double-differential cross sections give access to the self-inelastic structure factors for the $H_2$ centers of mass. Corrected experimental data, analyzed through the Young-Koppel model and the Gaussian approximation, are transformed into defect densities of phonon states, which come out to be broad, structured, and nearly concentration independent. Two experimentally determined Bose-corrected spectral moments are found to be in agreement with independent estimates, providing a strong validation of our data reduction procedure. Subsequently, experimental phonon spectra are compared to three calculations, namely, a simple harmonic model at infinite dilution, a more advanced harmonic model with concentration effects, and finally a lattice dynamics simulation based on self-consistent phonon and coherent potential approximations. However, while the first part of the defect spectral density, attributed to the propagating modes, turns out to be roughly explained, the localized part is properly described by none of these models, except for its mean frequency position. The large overall width appears so far impossible to be reproduced, representing a challenge for the physicists involved in quantum dynamics simulations.

DOI: 10.1103/PhysRevB.76.174304 PACS number(s): 63.20.−e, 67.80.Mg, 78.70.Nx

## I. INTRODUCTION

The lattice properties of the so-called quantum crystals ($^3$He, $^4$He, $H_2$, $D_2$, etc.) have been the subject of a large number of experimental investigations and theoretical studies.[1] However, despite the great advance in the understanding of these systems, some of their properties are still unclear, as proved by recent neutron scattering results on bcc $^4$He.[2] Moreover, if the theoretical point of view is considered, the achievements in describing quantum crystals appear even less satisfactory. It is true that the static properties of these solids (e.g., mean kinetic and potential energies, lattice constants, bulk modulus, etc.) seem reasonably well described by a number of quantum simulation methods, working either at zero temperature (such as *diffusion Monte Carlo*[3] and *Green function Monte Carlo*[4]) or at $T>0$ [such as *path integral Monte Carlo* (PIMC)].[5] However, as far as the quantum crystal lattice dynamics is concerned (i.e., phonon dispersion curves and density of phonon states), the scenario looks rather incomplete: the well-known *self-consistent phonon theory* is a pragmatic method to tackle these dynamic problems,[6] but it cannot be considered sufficiently general, and it has been recently shown that its prediction on the mean kinetic energy of high-density solid $^3$He is not very accurate.[7] On the other hand, the *path integral centroid dynamics*[8] and the *ring polymer molecular dynamics*[9] are relatively new and promising techniques, but surely need further development and a more rigorous theoretical validation, at least regarding the dynamic properties of quantum crystals. For example, in a recent study on solid para-hydrogen,[10] an accurate determination of the *density of phonon states* (DoPS) was extracted from inelastic neutron scattering spectra and compared to the most recent path integral centroid dynamics calculations.[11] An overall agreement was found, but yet a number of spectral shape details were missing or misplaced in the simulated data.

Given the aforementioned results on solid para-hydrogen, it was decided to continue the experimental studies on the self-dynamics of solid hydrogen isotopes, exploiting the intensity and the intrinsic incoherence of neutron scattering from para to ortho-hydrogen. In this scattering event, a para-hydrogen molecule in its rotational ground state ($J=0$, total nuclear spin $I=0$) is excited to an ortho-hydrogen molecule still in its rotational ground state ($J'=1$, total nuclear spin $I'=1$) through an inelastic collision with a neutron involving its spin flip. However, together with the rotational jump, the molecular center of mass can be either involved in no lattice excitation (elastic line), or in one lattice excitation (one phonon spectrum), or even in more excitations (multiphonon spectrum). One topic of particular relevance in this respect is the dynamics of $H_2$ defects in a solid $D_2$ matrix, where the phonon properties of a quantum crystal (i.e., solid $D_2$) are affected by the introduction of substitutional hydrogen impurities. Since the guest molecules are lighter than those of the host, they are supposed to vibrate with a frequency greater than any frequency of the $D_2$ lattice.[12] Such a mode cannot propagate through the crystal and the lattice vibration tends to be localized at the impurity site (localized modes). This situation, which is opposite to the one studied by Powell and Nielsen[13] (i.e., $D_2$ impurities in a $H_2$ crystal), shows some similarities with the problem of the $^3$He impurities in solid $^4$He.[14] However, the interpretation of the future experimental findings is simpler, since both the relatively high temperature of the lattice ($T>10$ K) and the bosonic nature of both $H_2$ and $D_2$ rule out completely any effects of the interplay between two opposite quantum statistics. In this way, the only

 

TABLE I. Thermodynamic conditions of the measured solid samples, including species, temperature $T$, $H_2$ molar concentration $c[H_2]$, total molecular density $n$, and integrated proton current IC.

| Sample | Species | $T$ (K) | $c[H_2]$ (%) | $n$ ($nm^{-3}$) | IC ($\mu$A h) |
|---|---|---|---|---|---|
| 1 | Pure n-$D_2$ | 14.10(5) | 0.0 | 30.03(1) | 2312.8 |
| 2 | n-$D_2$+p−$H_2$ | 13.15(1) | 3.7(4) | 29.91(2) | 2971.8 |
| 3 | n-$D_2$+p−$H_2$ | 13.68(9) | 6.5(4) | 29.74(2) | 4145.3 |
| 4 | n-$D_2$+p−$H_2$ | 13.63(8) | 10.2(4) | 29.56(2) | 3666.6 |
| 5 | Pure p-$H_2$ | 13.5(3) | 100.0 | 25.79(3) | 1177.1 |

difference in replacing $D_2$ with $H_2$ consists in the molecular mass (since the respective pair potentials are substantially identical[15]) and, from this, in the de Broglie wavelength, which measures the particle delocalization in the crystal lattice. Nevertheless, given the strong anharmonic character of quantum crystals, a simple mass substitution also produces a change in the coupling with its neighbors since the particle motions are strongly correlated and influence the effective coupling. So far, this effect, which makes the usual defect dynamics theories inapplicable to quantum crystals,[16] has been fully captured by the joint use of self-consistent phonon calculation and *coherent potential approximation*.[17] In this respect, the same limitations mentioned for the self-consistent phonon theory in pure systems apply to the diluted quantum alloys too. As for the cited coherent potential approximation, it is worth spending few words on its rationale: this is a quantum mechanical method devised to describe the electronic or phonon structures of substitutionally disordered solid systems.[18] The main point then consists in adding a suitable medium so that the "ensemble restricted average" of a host atom plus the "ensemble restricted average" of an impurity atom equal the average over the total ensemble. Such an ensemble restricted average can be thought as a configuration in which, e.g., a single host atom occupies a site in a lattice composed of averaged atoms.

The rest of the paper will be organized as follows. The experimental procedure will be described in detail in Sec. II. In Sec. III, we will work out the self-inelastic structure factor for para-hydrogen impurities in deuterium matrixes from the experimental spectra. In addition, we will obtain the $H_2$ density of phonon states by using the Gaussian approximation to estimate the unwanted multiphonon contributions. In Sec. IV, we will discuss the experimental results, and the physical quantities derived from the experimental spectra will be compared to their estimates obtained from the literature and from the original PIMC simulations. Section V will finally be devoted to conclusions and perspectives.

## II. EXPERIMENT DESCRIPTION

Neutron scattering measurements were carried out on TOSCA-II, a crystal-analyzer inverse-geometry spectrometer operating at the ISIS pulsed neutron source (Rutherford Appleton Laboratory, Chilton, Didcot, UK).[19] The incident neutron beam spanned a broad energy ($E_0$) range and the energy selection was carried out on the secondary neutron flight path using the (002) Bragg reflection of ten graphite single crystals, five placed in backscattering around a scattering angle of 137.7° and five in forward scattering around a scattering angle of 42.6°. This arrangement fixed the average Bragg angles on graphite to 47.7° and 47.4° (in backscattering and forward scattering, respectively), corresponding to scattered neutron energies of 3.32 and 3.35 meV. Higher-order Bragg reflections were filtered out by 120-mm-thick beryllium blocks, covered with cadmium and cooled down below 35 K. This geometry allowed to span an extended energy transfer range, even though the fixed positions of the crystal analyzers and the small values of the final neutron energy ($E_1$) imply a variation in the momentum transfer, $\hbar Q$, which is a function of the energy transfer $E$. In this way, the two parts of TOSCA-II (namely, the backscattering and forward scattering sections) explore two narrow stripes in the $(Q,E)$ kinematic space, starting at $E=0$, respectively, from $Q=23.61$ and 9.20 $nm^{-1}$, then both increasing approximately as $\sqrt{2m_nE/\hbar^2}$, where $m_n$ is the neutron mass. The resolving power of TOSCA-II is quite good ($1.5\% < \Delta E/E_0 < 3\%$) in the energy transfer region presently accessible by the spectrometer ($3 < E < 500$ meV). The extended spectral range of TOSCA-II makes this instrument a sort of neutron equivalent of a Raman optical spectrometer, the main difference being the momentum transfer assuming a value sensibly larger than zero and monotonically growing along with the energy shift.

The neutron measurements were performed in two different experimental sessions: the first was devoted to solid normal deuterium, pure, and mixed with para-hydrogen impurities (four thermodynamic points), while the second to pure solid para-hydrogen (one thermodynamic point). A comprehensive description of the sample measurements (including species, temperature, $H_2$ concentration, total molecular density, and integrated proton current) can be found in Table I.

Pressure measurements are not reported since they were ranging in all cases between the saturated vapor values and the upper limit of $p=0.11$ bar, so their effect on the sample densities was practically irrelevant. As far as the total molecular number density is concerned, the reported estimates were obtained from a collection of highly reliable[20] thermodynamic data available in the literature: Ref. 21 for pure para-hydrogen and Refs. 22 and 23 for pure normal deuterium, where the former study provided the ($T=0$, $p=0$) values and the latter the thermal expansion effect. Dealing with the three solid mixtures, the quoted molecular density values were obtained from the linear combination of the molar volumes of solid normal deuterium and solid para-hydrogen at

the corresponding temperature (ideal mixture), neglecting the excess mixing volume, which at $H_2$ concentrations between 4% and 10% can be estimated roughly as varying from −0.4% to −0.1%.[24] This is far below our level of accuracy on the sample densities, which is 0.7% (see Table I).

Another important issue is the total nuclear spin $I$ of the hydrogen and deuterium molecules composing the experimental samples, which, due to the Pauli principle, is linked with their rotational quantum number $J$. As it will be made clear later in this section, normal deuterium (11.1% of the $D_2$ molecules with $I=0$, 33.3% with $I=1$, and 55.6% with $I=2$) and para-hydrogen (all the $H_2$ molecules with $I=0$) have been employed. While the former is obtained simply by freezing room-temperature gas in the absence of microscopic magnetic fields, the latter was prepared from liquid hydrogen at $T=20$ K, where the equilibrium concentration of the para-species is greater than 99.82%,[25] the rest being composed of a tiny fraction of $I=1$ molecules (ortho-hydrogen). Nevertheless, even without paramagnetic impurities, the low-temperature solid phases of $H_2$ and $D_2$ present a slow spontaneous conversion to the least energetic state from the rotational point of view (i.e., $J=0$). Since this state is connected to $I=0$ in $H_2$ and to $I=0,2$ in $D_2$, one should observe the para-hydrogen content (already very high) to increase, and the normal deuterium fraction of the $D_2+H_2$ mixture to transform into ortho-deuterium (i.e., 16.7% of the molecules with $I=0$ and 83.3% with $I=2$), progressively altering the sample rotational composition. However, given the typical time scale of this process [namely, the exponential constant $K'=6.0\times10^{-4}$ $h^{-1}$ at $p=0$ and $T=4.2$ K (Ref. 26)] and the maximum acquisition time of the present neutron measurements (between 22 h for sample 3 and 44 h for sample 1), the spontaneous conversion effect can be safely ignored.

The first measurement was carried out on pure normal deuterium at $T=14.10$ K (i.e., on sample 1 as in Table I). After performing a background measurement of the empty cryostat, we cooled the sample container to low temperature (i.e., $T\leqslant20$ K) and we measured its neutron spectrum up to an integrated proton current IC=703.7 $\mu$A h. Then normal deuterium (99.995% chemically pure from Spectra Gases, Inc.) was allowed to condense at a pressure of about $p=0.61$ bar in the scattering cell kept at $T=22$ K. This was made of aluminum (2.0-mm-thick-walls) with a circular-slab geometry. The sample thickness was 2.5 mm and the cell diameter (60.0 mm) was slightly larger that the beam cross section ($40.0\times40.0$ $mm^2$). After filling up the cell volume with liquid, the sample was further cooled to the desired experimental temperature and then we started recording the scattering spectrum. The stability of the temperature during this measurement was satisfactory, being estimated around 0.05 K.

The second sample (namely, sample 2 at $T=13.15$ K) was a solid mixture of normal deuterium and para-hydrogen with $c[H_2]=3.7\%$ and was obtained in a different and more elaborated way with respect to sample 1. Let us summarize the main steps of the procedure followed to prepare this n-$D_2$ +p-$H_2$ alloy. Gaseous para-hydrogen (99.99% assay from BOC Gases Plc) and normal deuterium were produced boiling off the two liquids at 22 and 25 K, respectively, and then mixed in a buffer volume at room temperature under a pressure $p=2.14$ bar. The exact amount of gaseous mixture needed to fill up the sample cell (identical to the can already used for pure deuterium) with the corresponding liquid was allowed to condense in it (at $T=22$ K and $p=0.62$ bar). Then, the cell was cooled down to 11 K, so as to decrease the vapor pressure of the gas handling line to an extremely low value ($p\leqslant0.01$ bar). This step was regarded as very important in order to prevent an undesired separation of the mixture,[27] where the more volatile gas (i.e., p-$H_2$) could concentrate in the buffer volume, with the less volatile (i.e., n-$D_2$) condensed in the coldest point of the gas line, namely, in the sample cell. This would have altered the mixture composition in a quite noticeable way. At the end, the sample can was isolated from the rest of the gas handling line and warmed up to the requested experimental temperature (i.e., $T=13.15$ K). It is worth noting that the mixture was prepared and condensed on a time scale of an hour, regarded as too short to alter the $c[\text{p-}H_2]/c[H_2]$ ratio in a significant way. However, the possibility of small ortho-hydrogen contaminations ($c[\text{o-}H_2]/c[H_2]<5\%$) during the mixing procedure cannot be completely ruled out, and their effect in the narrow spectral region considered in rest of the present study (essentially between 14 and 35 meV) will be mentioned below. Samples labeled with 3 and 4 in Table I, characterized by $c[H_2]=6.5\%$ and 10.2%, respectively, were prepared and measured according to a procedure identical to that just described for sample 2.

The second session of the measurements, aiming to have a solid pure para-hydrogen measurement as a reference, was much simpler. We cooled the sample container to low temperature ($T<40$ K) and we shortly measured its neutron spectrum up to an integrated proton current of 177.7 $\mu$A h. Gaseous para-hydrogen (boiled off the liquid at $T=22$ K) was allowed to condense in the scattering cell kept at $T=17$ K. This was made of aluminum (1.0 mm thick walls) with a circular-slab geometry. The sample thickness was also 1.0 mm and the cell diameter was 55.0 mm. Then, sample 5 (namely, solid p-$H_2$ at $T=13.5$ K) was prepared simply by freezing the condensed liquid. The solidification was verified by monitoring the rotational line placed at $E=14.5$ meV through a series of short subruns: in solid p-$H_2$, this feature becomes on TOSCA-II extremely sharp and one order of magnitude higher than in the liquid, as clearly shown in Fig. 1 of Ref. 10. An integrated proton current of 1177.1 $\mu$A h was finally collected. The temperature conditions of all five samples were carefully chosen so that, even in the presence of some para-deuterium species (i.e., $I=1$ and $J=1$) like in samples 1–4, the crystal lattices always exhibited a hexagonal close-packed structure.[20]

All samples were in form of polycrystalline solid and were carefully checked by comparing spectra taken at similar values of the equatorial (scattering) angle $\theta$, but at completely different azimuthal angles $\phi$. No differences larger than the data statistical uncertainties were ever detected.

## III. DATA REDUCTION AND ANALYSIS

The experimental time-of-flight spectra were transformed into energy transfer data, detector by detector, making use of

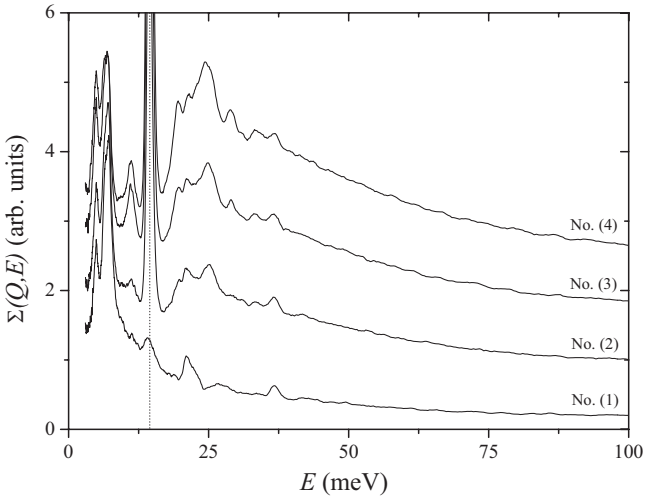


FIG. 1. Raw neutron scattering spectra from solid normal deuterium at $T=14.1$ K (sample 1) and from its mixtures with various amount of para-hydrogen (samples 2–4), ranging from 3.7% to 10.2%. Plotted data are from forward-scattering detectors and have been vertically shifted for graphic reasons (0.5 arbitrary units). Vertical dotted line around $E=14.5$ meV marks the intense $J=0\rightarrow J'=1$ rotational transition, which is out of scale.

the standard TOSCA-II routines available on the spectrometer and including the appropriate Waller-Froman Jacobian.[28] Then, the energy transfer spectra were focused in two distinct blocks: one including all the backscattering detectors and the other all the forward-scattering ones. This procedure was justified by the polycrystalline nature of the samples (i.e., no variation with the azimuthal angle $\phi$) and by the narrow angular range ($\theta$) spanned by each set of detectors, since the corresponding full widths at half maximum, $\Delta\theta$, were 8.32° and 8.82° for the backscattering and the forward-scattering banks, respectively.[19] In other words, all TOSCA-II detectors were placed at various values of $\phi$, but only at two possible values of $\theta$, namely, $\theta=43°\pm4°$ and $\theta=138°\pm4°$. In this way, we produced two double-differential cross-section measurements along the TOSCA-II kinematic paths $[Q_{F,B}(E),E]$ for each sample of Table I (plus, of course, background and empty cans). Then, data were corrected for the kinematic factor, $\sqrt{E_1/E_0}$, and the modest empty-can contributions were properly removed from each spectrum, taking into account the sample transmission as explained below. These spectra concerning samples 1–4 from forward-scattering detectors are reported in Fig. 1 before removing the empty can, but after correcting for the kinematic factor.

At this stage, the important correction for the *self-shielding* attenuation was performed. This was applied to experimental data through the analytical approach suggested by Agrawal and Sears in the case of a flat slablike sample:[29] no simplified model was employed for the deuterium total scattering cross section, $\sigma_{t,D_2}(E_0)$, which, on the contrary, was obtained from the experimental results of direct measurements on solid $D_2$ at $T=17$ K up to $E_0=80$ meV.[30] As for the total cross section of the $D_2+H_2$ mixtures, a proper linear combination of the aforementioned quantity $\sigma_{t,D_2}(E_0)$ with the total scattering cross sections of solid para-hydrogen (at $T=10$ K) (Ref. 30) was assumed to be accurate enough for the self-attenuation correction. The same total scattering cross section of p-$H_2$, $\sigma_{t,pH_2}(E_0)$, was also used to evaluate the self-attenuation in the pure solid para-hydrogen spectrum recorded on TOSCA-II.

The extraction of the p-$H_2$ DoPS in bulk solid and, as impurity, in solid deuterium matrices made use of the experimental data collected in forward scattering in the $14<E<40$ meV range. The preference for the forward-scattering data is simply justified, keeping in mind the asymptotic relationship[31] between the DoPS, $Z(\epsilon)$, and the spherically averaged self-dynamics structure factor, $S_s(Q,\epsilon)$, for a polycrystal with a cubic Bravaisian lattice, namely,

$$Z(\epsilon)_{\epsilon>0}=\lim_{Q\rightarrow 0}\left\{S_s(Q,\epsilon)\frac{4M\epsilon}{\hbar^2Q^2}\exp[2W(Q)]\times\left[\coth\left(\frac{\epsilon}{2k_BT}\right)+1\right]^{-1}\right\}, \quad (1)$$

where $2W(Q)$ is the well-known Debye-Waller factor and $\epsilon$ denotes the center-of-mass energy (to prevent ambiguities with the energy transfer $E$). Of course, we are not able to perform any direct $Q\rightarrow 0$ extrapolation in our experimental kinematic conditions, and so we will need a more elaborated procedure in order to work out $Z(\epsilon)$. However, choosing the lowest $Q$ values available is always a recommendable practice in the extraction of the DoPS, since at high $Q$ values the relevant one-phonon features are often masked and swamped by multiphonon contributions.

Going back to the forward-scattering experimental data for the $n$th sample (already corrected for $\sqrt{E_1/E_0}$, container scattering, and self-attenuation), after normalizing them to reference sample thickness and density, one notes that they can be considered as proportional to the sum of a *generalized scattering law* $\Sigma^{(n)}(Q,E)$, which simply reads

$$\Sigma^{(n)}(Q,E)=\sqrt{\frac{E_0}{E_1}}\left(\frac{d^2\sigma}{d\Omega dE_1}\right)^{(n)}, \quad (2)$$

plus $M^{(n)}(Q,E)$, which contains all the various multiple scattering contributions. It is worthwhile to remind that the dependence on the **Q** orientation is neglected here (and it will be also in what follows), given the polycrystalline character of all the samples involved.

At this stage, it is convenient to introduce the $D_2$-subtracted data, $\tilde{\Sigma}^{(n)}(Q,E)$,

$$\tilde{\Sigma}^{(n)}(Q,E)=\Sigma^{(n)}(Q,E)-(1-c^{(n)}[H_2])\Sigma^{(1)}(Q,E). \quad (3)$$

Using the same approach employed in the study of liquid hydrogen-deuterium mixtures,[32] one can safely neglect all the residual distinct and diffuse scattering terms and approximate $\tilde{\Sigma}^{(n)}(Q,E)$ as

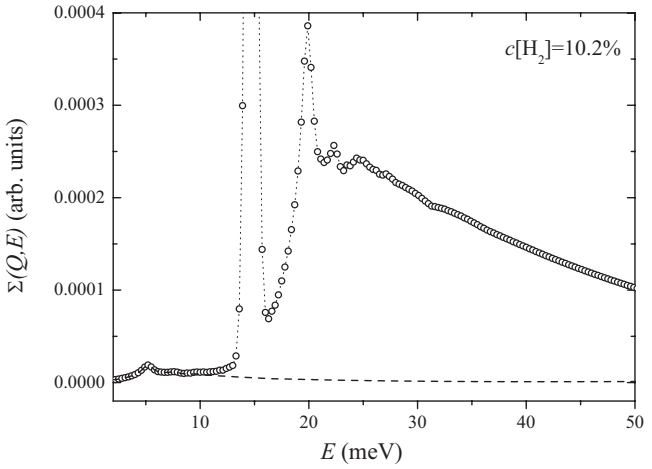


FIG. 2. Approximate simulation of the p-$H_2$ incoherent contributions to the generalized scattering law (assuming a para-hydrogen concentration of 10.2% as in sample 4). The sum of the p-$H_2$ rotational self-terms is plotted as empty circles and dotted line, while the same quantity minus the term related to the $J=0\rightarrow J'=1$ transition is also reported separately as dashed line.

$$\tilde{\Sigma}^{(n)}(Q,E) \simeq c^{(n)}[\mathrm{H}_2] \sum_{J' \geq 0} \Sigma_{J'}^{(n,\mathrm{pH}_2)}(Q,E), \tag{4}$$

where the various rotational self-contributions, $\Sigma_{J'}^{(n,\mathrm{pH}_2)} \times(Q,E)$, labeled with the final rotational quantum number $J'$, have been made explicit. Looking at Fig. 2, where $c^{(n)}[\mathrm{H}_2]\Sigma_{J'=1}^{(n,\mathrm{pH}_2)}(Q,E)$ has been plotted separately from the sum of all the other terms included in $\tilde{\Sigma}^{(n)}(Q,E)$, one can conclude that in our kinematic range of interest, the only relevant term is the $J=0\rightarrow J'=1$ one,

$$\tilde{\Sigma}^{(n)}(Q,E) \simeq c^{(n)}[\mathrm{H}_2]\Sigma_{J'=1}^{(n,\mathrm{pH}_2)}(Q,E) = c^{(n)}[\mathrm{H}_2]4\frac{\sigma_{i,\mathrm{H}}}{4\pi} \times \exp[-2W_v(Q)]j_1^2(Qr_e/2)S_s(Q,E-E_{0-1}). \tag{5}$$

In the last line of the above equation, the well-known Young-Koppel[33,34] model has been employed, where $\sigma_{i,\mathrm{H}}$ is the H incoherent scattering cross section,[31] $\exp[-2W_v(Q)]$ is the intramolecular vibrational Debye-Waller factor for $H_2$,[33] $j_1(x)$ is the spherical Bessel function of first order, $r_e$ is the equilibrium intramolecular distance in $H_2$, $S_s(Q,\epsilon)$ is the self-inelastic structure factor for the $H_2$ centers of mass[31] (spherically averaged because of the polycrystalline samples), and $E_{0-1}$ is the energy shift for the $J=0\rightarrow J'=1$ transition.

Dealing now with the multiple scattering contamination, first one has to note that the subtraction of the deuterium contribution in Eq. (3) has also affected $M^{(n)}(Q,E)$, which has been automatically replaced by $\tilde{M}^{(n)}(Q,E)$,

$$\tilde{M}^{(n)}(Q,E) = M^{(n)}(Q,E) - (1-c^{(n)}[\mathrm{H}_2])M^{(1)}(Q,E). \tag{6}$$

This new multiple scattering spectrum was accurately simulated through the analytical approach by Agrawal and Sears,[29] in conjunction with the incoherent approximation,[35] the modified Young-Koppel model for both $H_2$ and $D_2$,[33,34] and the Gaussian approximation for the molecular center of mass dynamics.[36] Following the various steps of the calculation, we can sketch the entire procedure in three main points.

(1) Use two model DoPS's for the host (n-$D_2$) and the impurity (p-$H_2$) to generate the respective self-center-of-mass scattering laws in an appropriate portion of the kinematic plane $(Q,E)$ through the mentioned Gaussian approximation. It has been verified that the following rectangular zone was sufficiently large for our purposes: $Q<440$ nm$^{-1}$ and $-3.3$ meV$<E<1$ eV.

(2) Apply the modified Young-Koppel model to transform the self-center-of-mass scattering laws into the sample double-differential cross section including the rotational dynamics of both n-$D_2$ and p-$H_2$ through appropriate convolutions. The first eight rotational levels of n-$D_2$, $0\leqslant J'\leqslant 7$, have been considered in the calculation;

(3) Implement the cited formulas by Agrawal (double scattering) and by Sears (higher order terms) in the case of a flat slab, making use of the energy dependent self-attenuation factors already evaluated. This final step has been accomplished through a computer code[37] especially set up for inverse-geometry machines such as TOSCA-II.

To sum up, the only needed input data were the DoPS's for bulk solid deuterium (taken from Ref. 38 and properly scaled to the present sample density) and for para-hydrogen embedded in n-$D_2$ matrixes. The latter quantity, whose extraction is actually the main aim of the present study, was approximately obtained from a preliminary version of data analysis in which the multiple scattering correction had been operated in a cruder way. The stability of the simulation results was checked by replacing these preliminary p-$H_2$ DoPS's by the final ones extracted from the present measurements (see below) and observing no noticeable change in the multiple scattering spectra. An example from sample 4 is reported in Fig. 3 in the energy transfer range of interest.

It is evident that the multiple scattering contribution $\tilde{M}^{(4)}(Q,E)$ was not at all irrelevant (being about 33% of the total scattering between 14 and 40 meV after removing the n-$D_2$ signal), but luckily it exhibits in this region a series of corrugations quite smaller than the main single scattering features, giving rise to a sort of background. In addition, the ridges in the $\tilde{M}^{(4)}(Q,E)$ contribution corresponded almost exactly to the peaks in the single scattering spectrum since on TOSCA-II, a large portion of multiple scattering is generally originated by the combination of one single inelastic event plus one (or more) elastic event(s), as explained in Ref. 37. Appropriate multiple scattering contributions were finally subtracted from samples 2–4 data sets, which in this way became proportional to $\Sigma_{J'=1}^{(n,\mathrm{pH}_2)}(Q,E)$. These experimental spectra were further corrected according to Eq. (5), in order to single out experimental estimates of $S_s(Q,E-E_{0-1})$, reported in Fig. 4, evaluated along the forward-scattering

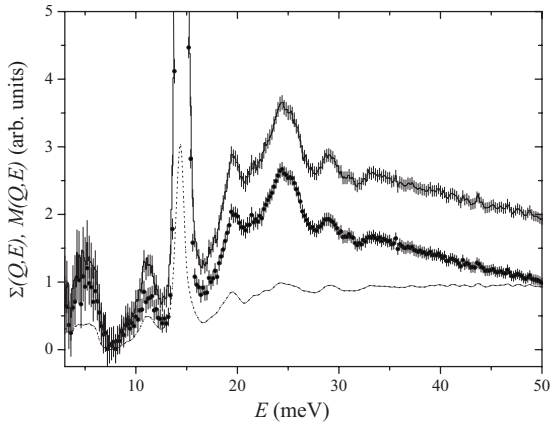


FIG. 3. Example of the multiple scattering correction applied to sample 4 (after subtracting the pure deuterium spectrum). Full line with error bars represents the uncorrected spectrum, dotted line stands for the multiple scattering contribution $\tilde{M}^{(4)}(Q,E)$, and their difference, $\tilde{\Sigma}^{(4)}_{J'=1}(Q,E)$ (i.e., the single scattering contribution), is reported as full circles with error bars.

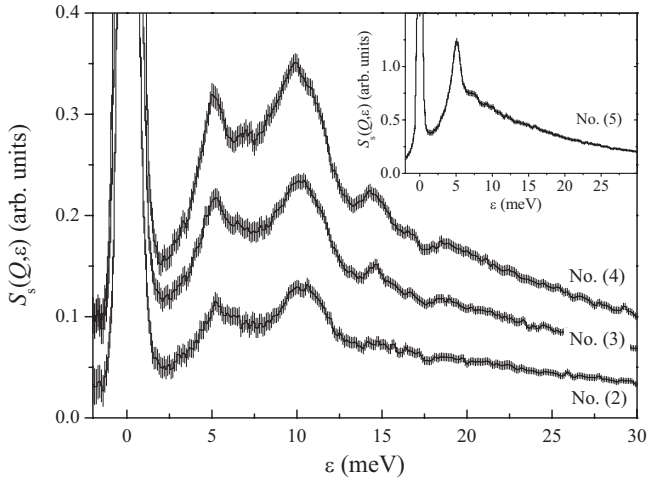


FIG. 4. $H_2$ center-of-mass self-scattering law, $S_s(Q_F,\epsilon)$, from mixtures with various amount of para-hydrogen (samples 2–4), ranging from 3.7% to 10.2%. The sharp peak around $\epsilon=0$ (out of the plot range) represents the elastic line. In the inset, we have reported the same quantity for pure bulk para-hydrogen (sample 5) as a comparison.

TOSCA-II trajectory $Q=Q_F(E)$ and broadened by the instrumental resolution, $\Delta E(E)$. Details about the energy shift $E_{0-1}$ removal (i.e., $\epsilon=E-E_{0-1}$) are given below.

The self-inelastic structure factor for the p-$H_2$ centers of mass was analyzed, making use of the Gaussian isotropic approximation[35,36] for $S_s(Q,\epsilon)$,

$$S_s(Q,\epsilon) = \exp[-2W_l(Q)]\int_{-\infty}^{\infty}\frac{dt}{2\pi\hbar}\exp(-i\hbar^{-1}\epsilon t) \times\exp\left\{-\frac{\hbar^2Q^2}{2M}\int_{-\infty}^{\infty}f_p(\epsilon')[\cos(\hbar^{-1}\epsilon' t) + i\sin(\hbar^{-1}\epsilon' t)]d\epsilon'\right\}, \quad (7)$$

where $M$ is the molecular mass, $f_p(\epsilon)$ is the phonon spectral density, and $\exp[-2W_l(Q)]$ is the lattice Debye-Waller factor for the p-$H_2$ centers of mass, which is simply related to $f_p(\epsilon)$ via

$$W_l(Q) = \frac{\hbar^2Q^2}{4M}\int_{-\infty}^{\infty}d\epsilon f_p(\epsilon). \quad (8)$$

It is to point out that, for a lattice, the previous equation assumes its exact validity only in the cases of a polycrystalline (i.e., powder averaged) cubic and harmonic crystal. On one side, no dependence on the **Q** direction was assumed anywhere, and, on the other side, the well-known Bloch formula[31] was used. Actually, our p-$H_2$ impurity sample is, strictly speaking, neither polycrystalline cubic (having an hcp structure) nor perfectly harmonic (being a quantum crystal). However, as for the first point, it is to note that the local environment of an $H_2$ molecule in an hcp $D_2$ lattice is not strongly anisotropic, being identical to an fcc one up to the second neighbors' shell. As for the harmonicity, it has been shown by Horner[39] and Glyde[40] that Eq. (7) is still approximately applicable to a quantum solid, as experimentally confirmed in the case of solid para-hydrogen by Bickermann *et al.*[41] and Colognesi *et al.*[10] In practice, in a quantum solid one has to correct the link between the phonon spectral density, $f_p(\epsilon)$, and the DoPS, $Z(\epsilon)$, counting of the phonons in a certain $\epsilon$ interval,[31] by introducing anharmonic phonon damping and renormalization. Following the approach outlined in Refs. 42 and 43, it is customary to write

$$f_p(\epsilon) = \frac{1}{6N}\sum_{\mathbf{q},j}^{6N}\frac{A(\mathbf{q},j;\epsilon)}{2\pi\hbar\omega(\mathbf{q},j)}\frac{1}{1-\exp[-\hbar\omega(\mathbf{q},j)/k_BT]}, \quad (9)$$

where $\mathbf{q}$ is a phonon wave vector contained in the first Brillouin zone (FBZ) of the crystal, $N$ the number of wave vectors in the FBZ, $j$ labels the six phonon branches of an hcp lattice, $\omega(\mathbf{q},j)$ is the phonon frequency, and $A(\mathbf{q},j;\epsilon)$ is the so-called *anharmonic one-phonon response function* approximately expressed by

$$A(\mathbf{q},j;\epsilon) \simeq \frac{8\hbar\omega(\mathbf{q},j)\epsilon\Gamma(\mathbf{q},j)}{[\hbar^2\omega^2(\mathbf{q},j)-\epsilon^2+2\hbar\omega(\mathbf{q},j)\Delta(\mathbf{q},j)]^2+2\hbar\omega(\mathbf{q},j)\epsilon\Gamma^2(\mathbf{q},j)}, \quad (10)$$

TABLE II. Physical quantities related to the $H_2$ impurity samples, including mean squared displacement of the molecular center of mass, $\langle \mathbf{u}^2 \rangle$, derived from the elastic line; elastic line mean position (plus the $E_{0-1}$ value) $m_F$; elastic line intrinsic broadening $\sqrt{\tilde{v}_F}$; mean squared displacement of the molecular center of mass, $\langle \mathbf{u}^2 \rangle_{in}$, derived from the experimental phonon distribution integral; center-of-mass mean kinetic energy, $\langle E_k \rangle_{in}$, derived from the experimental phonon distribution integral; and center-of-mass mean kinetic energy, $\langle E_k \rangle_{\mathrm{PIMC}}$, derived from quantum simulations.

| Sample | $\langle \mathbf{u}^2 \rangle$ (Å$^2$) | $m_F$ (meV) | $\sqrt{\tilde{v}_F}$ (meV) | $\langle \mathbf{u}^2 \rangle_{in}$ (Å$^2$) | $\langle E_k \rangle_{in}$ (K) | $\langle E_k \rangle_{\mathrm{PIMC}}$ (K) |
|---|---|---|---|---|---|---|
| 2 | 0.41(2) | 14.43(3) | 0.41(4) | 0.426(9) | 86(4) | 86.7(3) |
| 3 | 0.46(1) | 14.44(3) | 0.42(4) | 0.457(4) | 84(2) | 85.5(3) |
| 4 | 0.45(1) | 14.44(3) | 0.38(4) | 0.443(2) | 85(2) | 85.7(1) |

where $\Delta$ and $\hbar\Gamma^{-1}$ are the phonon energy shift and lifetime, respectively, due to anharmonicity. However, in the rest of the paper, we will often make use of an *effective anharmonic density of phonon states* (EA-DoPS), $\tilde{Z}(\epsilon)$, defined for $\epsilon > 0$ as

$$\tilde{Z}(\epsilon) = f_p(\epsilon)\epsilon(1 - e^{-\epsilon/k_B T}) = \frac{1}{6N}\sum_{\mathbf{q},j}^{6N} \frac{\epsilon A(\mathbf{q},j;\epsilon)}{2\pi\hbar\omega(\mathbf{q},j)} \frac{1 - \exp(-\epsilon/k_B T)}{1 - \exp[-\hbar\omega(\mathbf{q},j)/k_B T]}, \quad (11)$$

which coincides with the usual $Z(\epsilon)$ in the harmonic limit: $\Gamma \to 0$ and $\Delta \to 0$. In addition, it is possible to prove that $\tilde{Z}(\epsilon)$ is exactly equal to the spectral function $\hbar^{-1} f(\omega)$, defined by Rahman *et al.*,[36] which has a straightforward physical meaning, being related to the Fourier transform of the imaginary part of the time-velocity autocorrelation function. Moreover, it satisfies various important sum rules, e.g., it is rigorously normalized to the unity and its Bose-corrected first moment is proportional to the single-particle mean kinetic energy,[36] as we will see later.

Experimental $S_s(Q_F, \epsilon)$ data were subsequently removed of the intense elastic line, fitted in the narrow energy-transfer range $-1.5 < \epsilon < 1.7$ meV and then analyzed separately. Fits were performed using a sum of two Gaussian curves (six free parameters) plus a small linear background (other two free parameters) to account for the onset of the inelastic part. This procedure was performed on both forward-scattering and backscattering data (the latter being processed in a similar way as the former), so as to obtain peak parameters at two different wave-vector transfer values: $Q_F(E_{0-1})$ and $Q_B(E_{0-1})$.

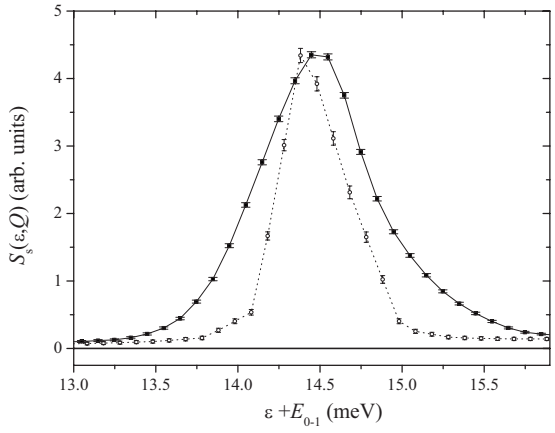


FIG. 5. Experimental determination of the elastic line in the self-dynamic structure factor for the $H_2$ centers of mass from samples 4 (full line with full squares) and pure para-hydrogen (sample 5) (dotted line with empty circles). The latter spectrum has been properly scaled to show the same height as the former.

Pure para-hydrogen data [i.e., sample 5], reported in the inset of Fig. 4, were also taken into account after a data analysis identical to that reported in Ref. 10, where the DoPS is extracted and compared to various simulations. Here, it is not important to provide long details about the solid p-$H_2$ phonon spectrum, but is worth mentioning the characteristic strong peak placed at about $\epsilon = 5$ meV, due to the intersection of the transverse acoustic phonon branches with the boundary of the first Brillouin zone.[23] The importance of the pure para-hydrogen measurements in the present context will be made clear later.

From the best-fitted parameters, peak areas $A_{F,B}^{(2-5)}$, means $m_{F,B}^{(2-5)}$, and variances $v_{F,B}^{(2-5)}$, were easily estimated and used for further analyses. Using the Debye-Waller factor for pure p-$H_2$ at low pressure and $T = 13.3$ K (namely, $\langle \mathbf{u}^2 \rangle^{(5)} = 0.53(2)$ Å$^2$, as in Ref. 10), the relative detector bank efficiency $\eta$ between forward-scattering and backscattering data was evaluated using the formula

$$\eta = \frac{A_F^{(5)}}{A_B^{(5)}} \frac{\exp\{-2W_l^{(5)}[Q_B(E_{0-1})]\}}{\exp\{-2W_l^{(5)}[Q_F(E_{0-1})]\}} = 0.95(7), \quad (12)$$

where the simple isotropic and pseudoharmonic approximation implied by Eq. (8) was assumed: $2W_l(Q) = \langle \mathbf{u}^2 \rangle Q^2/3$. Then, it was possible, from $A_{F,B}^{(2-4)}$, to extract reliable estimates of mean squared displacement of the $H_2$ center of mass, $\langle \mathbf{u}^2 \rangle^{(2-4)}$, listed in Table II. A similar approach was used to study the broadening of the $J = 0 \to J' = 1$ lines caused by the presence of para-deuterium neighbors (see Fig. 5): since the intrinsic broadening of this rotational line in pure bulk para-hydrogen is really tiny ($\sim 0.01$ cm$^{-1}$),[26] $v_F^{(5)}$ was assumed to be caused by the instrumental resolution alone and then removed from the other variances: $\tilde{v}_F^{(2-4)} = v_F^{(2-4)} - v_F^{(5)}$, so as to obtain reliable intrinsic rotational broadening values for samples 2–4, reported in Table II. Finally, the

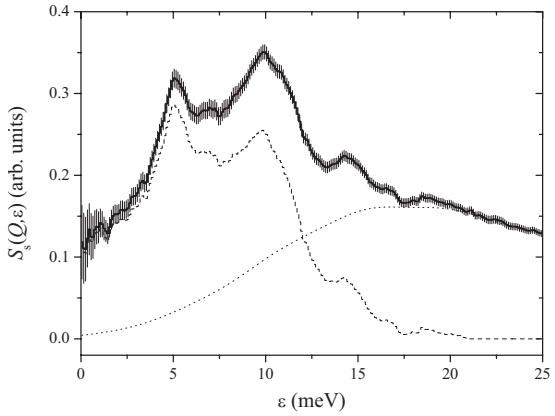


FIG. 6. Experimental self-dynamic structure factor for the $H_2$ centers of mass in sample 4 (full line with error bars), self-consistent evaluation of its multiphonon contribution (dotted line), and their difference (dashed line), i.e., the one-phonon component.

fitted values $m_F^{(2-5)}$ were used to operate an accurate energy shift from $E$ to $\epsilon=E-E_{0-1}$.

Thus, the last stage before the extraction of the EA-DoPS was the evaluation and the subtraction of the multiphonon contribution, not totally negligible because of the $Q$ values attained by TOSCA-II in the $14<E<40$ meV range (namely, from 21.4 to 37.4 $nm^{-1}$). The inelastic part of $S_s(Q_F,\epsilon)$ was processed through an iterative self-consistent procedure[44] in the range $0<\epsilon<25$ meV, aiming to extract the one-phonon component of the self-scattering law for the p-$H_2$ centers of mass, i.e., $S_s^{(1)}(Q,\epsilon)$ (see Fig. 6). All the technicalities of this method can be found in Ref. 37.

Finally, from $S_s^{(1)}(Q,\epsilon)$, the phonon spectral density, $f_p(\epsilon)$, was simply worked out via[35]

$$f_p(\epsilon)=\exp[2W_l(Q)]S_s^{(1)}(Q,\epsilon)\frac{2M}{\hbar^2Q^2}, \tag{13}$$

together with Eq. (8), and then plotted in Fig. 7 in the form of $\tilde{Z}_H(\epsilon)$, the effective anharmonic density of phonon states for the $H_2$ defects.

## IV. DISCUSSION

The first results to be discussed concern the width of the elastic lines in $S_s(Q_F,\epsilon)$ [actually being the $J=0\rightarrow J'=1$ lines in $\Sigma_{J'=1}^{(n,\mathrm{pH_2})}(Q,E)$], which, as explained in the previous section, have been fitted and then subtracted from the $S_s(Q_F,\epsilon)$ experimental data. The elastic line intrinsic broadening values, $\sqrt{\tilde{v}_F^{(2-4)}}$ (see Table II), have to be compared with the predictions coming from the theory of anisotropic interactions in solid hydrogen,[45] namely, the splitting effect of the para-deuterium neighbors (with $J=1$) on the final state (labeled with $J'=1$) of the $H_2$ molecule hit by the neutron.

Following Refs. 26 and 46, one can write

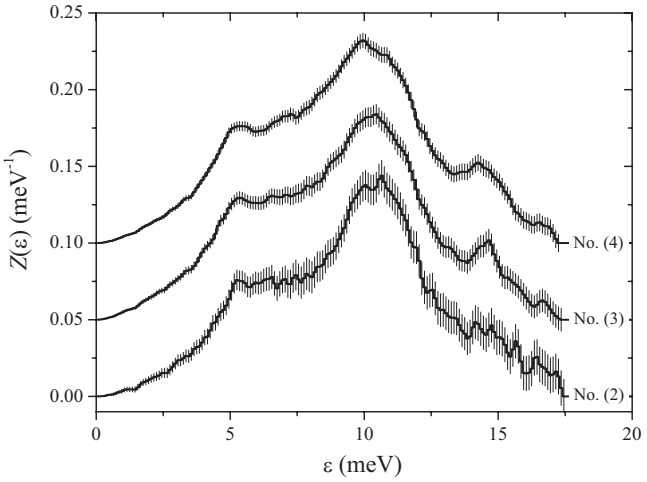


FIG. 7. Experimental (effective anharmonic) densities of phonon states, $\tilde{Z}(\epsilon)$, from mixtures with various amount of para-hydrogen (samples 2–4), ranging from 3.7% to 10.2%. Plots have been vertically shifted for graphic reasons (by 0.05 $meV^{-1}$).

$$\tilde{v}^{(n)}=\frac{35}{1250}\left(\frac{c[\mathrm{p-D_2}]}{c[\mathrm{D_2}]}\right)(1-c^{(n)}[\mathrm{H_2}])\sqrt{\xi(\mathrm{H_2})\xi(\mathrm{D_2})}\times Q_e(\mathrm{D_2})^2Q_e(\mathrm{H_2})^2\left\langle\sum_j R_{ij}^{-10}\right\rangle, \tag{14}$$

where $\left(\frac{c[\mathrm{p-D_2}]}{c[\mathrm{D_2}]}\right)=1/3$ is the relative abundance of $J=1$ species in low-temperature normal deuterium, $Q_e$ is the permanent quadrupole moment of a molecule, $\langle\Sigma_j R_{ij}^{-10}\rangle$ is the lattice sum of the intermolecular average distances to the power of $-10$, and $\xi$ is the solid reduction factor, which takes approximately into account both the molecular dynamical correlation in the lattice sum and the effects beyond the quadrupole-quadrupole interaction (i.e., quadrupole–van der Waals and quadrupole-valence). Plugging the most recent estimates of the aforementioned physical quantities into Eq. (14), one obtains the theoretical values of the $J=0\rightarrow J'=1$ intrinsic broadening in our samples, namely, $\sqrt{\tilde{v}^{(2-4)}}=0.490$, 0.478, and 0.464 meV, respectively, for samples 2, 3, and 4. These figures show a fairly good agreement with the experimental values in Table II, even though the theory exhibits an overestimate of about 17% with respect to 10%-accurate experimental data. Before concluding this subject, it is important to stress that this intrinsic rotational broadening due to the splitting of the $H_2$ final state with $J'=1$ is not limited in $S_s(Q_F,\epsilon)$ to the elastic line, but, on the contrary, affects the whole spectral function, behaving like a sort of additional energy resolution to be added to the instrumental one, giving rise to an effective value worse than the nominal TOSCA-II one.

Moving to the phonon part of the measurements, i.e., $\tilde{Z}(\epsilon)$ (reported in Fig. 7), one can immediately observe the strong similarity among the three effective densities of phonon states, which practically coincide within the error bars. This is an important result showing that, at the present level of effective energy resolution [i.e., full width at half maximum

(FWHM), $\Delta E \simeq 1$ meV], the localized phonon modes of $H_2$ in a deuterium matrix do not show any relevant concentration effect from $c[H_2] \simeq 4\%$ up to 10% (with the possible exception of the $14 \text{ meV} < \epsilon < 16$ meV zone). However, given the elaborate data analysis procedure described in Sec. III, it is useful to validate the extracted $\tilde{Z}(\epsilon)$ before proceeding with a further discussion. Two physical quantities related to the $H_2$ center of mass vibrations can be used to this aim: the mean squared displacement $\langle \mathbf{u}^2 \rangle$ and the mean kinetic energy $\langle E_k \rangle$. An inelastic ("in") estimate of the former was obtained from $\tilde{Z}(\epsilon)$, using Eq. (8), while the latter was given by[36]

$$\langle E_k \rangle_{in} = \frac{3}{4} \int_0^\infty \epsilon \tilde{Z}(\epsilon) \coth\left(\frac{\epsilon}{k_B T}\right) d\epsilon, \tag{15}$$

where only the isotropic approximation (not the pseudoharmonic one) has been assumed.[36] Inelastic estimates of mean squared displacements $\langle \mathbf{u}^2 \rangle_{in}$ and mean kinetic energies $\langle E_k \rangle_{in}$ are reported in Table II where can be compared with independent evaluations of the same quantities: $\langle \mathbf{u}^2 \rangle$ derived from the elastic line in the previous section and $\langle E_k \rangle_{\text{PIMC}}$ obtained from original PIMC simulations. The agreement between the two data sets, both for mean squared displacement and mean kinetic energy, is totally satisfactory and represents a stringent assessment on the reliability of the data analysis procedure since these two physical quantities are mainly sensitive to different parts of $\tilde{Z}(\epsilon)$, namely, to the low-$\epsilon$ and to the high-$\epsilon$ portions of the phonon spectrum, respectively.

As for the PIMC calculations, it is worth spending a few more words on the procedure employed to simulate solid pure $D_2$ and $D_2+H_2$ mixtures: an *NVT* (i.e., isochoric-isothermal) PIMC code was used setting molecular density ($n=N/V$) and temperature $T$ to values identical to those reported in Table I. As for the hydrogen concentration, the $c[H_2]$ values were slightly altered according to the following list: 3.645 $8\bar{3}$%, 6.25%, and 10.156 25%, respectively, for samples 2, 3, and 4. Simulations were carried out using the semiempirical isotropic pair potential derived by Silvera and Goldman[15] and still considered one of the most reliable for para-$H_2$ and ortho-$D_2$ in low-temperature condensed phases. The anisotropic pair potential components, present because of the para-$D_2$ population in n-$D_2$, were actually neglected because of their relative smallness with respect to the large isotropic part.[47] Hydrogen defects were inserted into the hcp crystal lattice by replacing deuterium molecules through a fully random distribution. The PIMC algorithm was then accomplished by extending the number of monomers (the so-called *Trotter number P*) of $N=384$ ringlike polymers, which in the PIMC isomorphism[5] represent the quantum particles of $D_2$ (or $H_2$), from $P=12$ to 25 and 50. However, only tiny differences were observed between $P=25$ and $P=50$ results for both mean kinetic energy and virial coefficient, proving the actual convergence of the algorithm at $P=50$. This code has been already successfully employed in a number of simulations on solid para-$H_2$,[48] on liquid ortho-$D_2$,[49] and liquid mixtures of para-$H_2$ and ortho-$D_2$.[32] Further details on this kind of simulations can be found in the aforementioned references on the code usage.

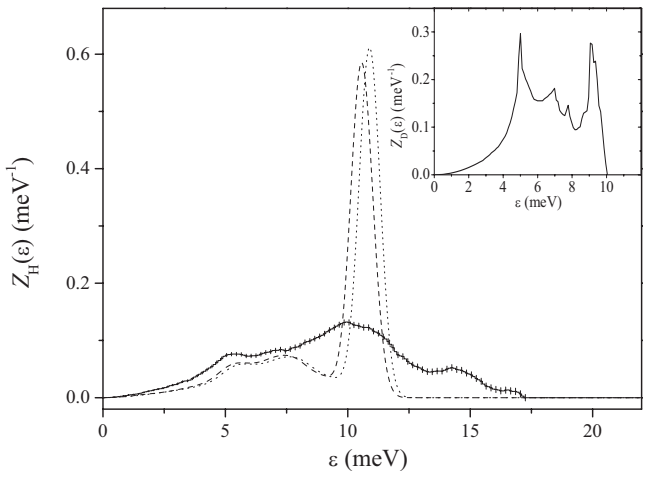


FIG. 8. Experimental (full line plus error bars) and theoretical harmonic estimates of the hydrogen-defect density of phonon states in a solid deuterium matrix for sample 4. Dotted line is obtained from a simple single-impurity theory (Ref. 51), while dashed line represents the result of a more advanced calculation (Ref. 52). The inset (upper right corner) reports the pure solid deuterium density of phonon states derived from Ref. 38.

So far, we have basically discussed only some equilibrium properties of the $H_2$ defects embedded in solid $D_2$ matrixes, e.g., the mean squared displacement and mean kinetic energy of the molecular centers of mass. Let us focus now on the dynamical features captured by the experimentally extracted EA-DoPS. In order to understand the physical meaning of the curves reported in Fig. 7, it is useful to start from the phonon distribution in pure bulk solid $D_2$. Unfortunately, the information on this physical quantity is very limited, since deuterium exhibits a relevant coherent neutron scattering cross section, which makes the direct extraction of the DoPS an impossible task. However, a semiexperimental DoPS evaluation has been obtained from the measured phonon dispersion curves fitted by a Born–von Kármán force constant model, making use of the Gilat-Raubenheimer method.[38] This estimate, slightly rescaled via an average Grüneisen parameter[50] [$\gamma=1.88$ (Ref. 38)] to match our experimental density (i.e., that of sample 1), is reported in the inset of Fig. 8.

It is important to stress that this curve, which intrinsically contains no phonon damping at all and an unknown quantity of anharmonic phonon shift, has to be meant more as a pseudoharmonic $Z(\epsilon)$ (Ref. 31) than as a fully EA-DoPS $\tilde{Z}(\epsilon)$ [see Eq. (11)]. It exhibits a clear cutoff energy, $\epsilon_{c-o} \simeq 10$ meV. Unperturbed deuterium DoPS's from Ref. 38, once again slightly corrected for the effective sample densities, $Z_D^{(n=2-5)}(\epsilon)$, were then employed to evaluate the $H_2$ defect density of phonon states $Z_H^{(n=2-5)}(\epsilon)$, using the standard harmonic theory[12] based on a Dyson equation for the lattice Green function. In its simplest version, strictly rigorous only for a single impurity in a Bravaisian cubic lattice, one obtains a $Z_H^{(n)}(\epsilon)$ which can be written[51] as the sum of a propa-

gating part [with the same range as $Z_{\mathrm{D}}^{(n)}(\epsilon)$], plus a single localized energy value $\epsilon_l^{(n)}$ (always larger than $\epsilon_{c-o}$). It is convenient to express the propagating part as the product of the host DoPS, $Z_{\mathrm{D}}^{(n)}(\epsilon)$, divided by a distortion function $D^{(n)}(\epsilon)$, and finally rescaled by the ratio of the host mass to the impurity one. The localized component is expressed by a delta function centered in $\epsilon=\epsilon_l^{(n)}$ times a constant $h^{(n)}$ so to normalize the total $Z_{\mathrm{H}}^{(n)}(\epsilon)$. Putting the two terms together, one writes

$$Z_{\mathrm{H}}^{(n)}(\epsilon)=\frac{M_D}{M_H}\frac{Z_{\mathrm{D}}^{(n)}(\epsilon)}{D^{(n)}(\epsilon)}+h^{(n)}\delta(\epsilon-\epsilon_l^{(n)}), \tag{16}$$

where $\epsilon_l^{(n)}$, $D^{(n)}(\epsilon)$, and $h^{(n)}$ depend only on $Z_{\mathrm{D}}^{(2-5)}(\epsilon)$ and $\lambda$ (with $\lambda=1-M_H/M_D$), and their definitions can found in detail in Ref. 51 together with an efficient numerical method to evaluate them. The calculation of $Z_{\mathrm{H}}^{(4)}(\epsilon)$ (i.e., for sample 4), convoluted with appropriate instrumental resolution and intrinsic rotational broadening, is reported in Fig. 8 together with the corresponding experimental data. A quick inspection already reveals a poor agreement between experimental $\tilde{Z}(\epsilon)$ and simulated $Z_{\mathrm{H}}^{(4)}(\epsilon)$, and this is not surprising at all given the purely harmonic character of the theory,[16] as we have explained in the Introduction. However, a more careful observation of the aforementioned figure exhibits some interesting features: the low-energy simulated DoPS portion (up to 10 meV), though less intense and slightly shifted to the right, is not at all far from the experimental data and shows the same Debye-like onset and double-hump structure caused by the main acoustic and optical branches in the $D_2$ DoPS (see inset in Fig. 8). In addition, the $\epsilon_l^{(4)}$ localized mode, which in our simple theory is a single energy value, comes spontaneously quite close to the maximum of the experimental $\tilde{Z}(\epsilon)$, being placed, respectively, at 10.88 and at 9.95 meV.

In the calculation we have just presented, the role of the $H_2$ defect concentration is explicitly absent, being indirectly involved only in the small density corrections operated on $Z_{\mathrm{D}}^{(n)}(\epsilon)$ via the average Grüneisen parameter.[50] However, a more advanced theory dealing with finite defect concentrations has been developed,[52] although still in the framework of the harmonic approximation. The calculations are far more demanding since the well-known $t$ matrix (describing phonon scattering from impurities) has now to be evaluated, at least within the isotropic approximation. The main qualitative difference between these two theories lies in the fact that the single value $\epsilon_l^{(n)}$ in Eq. (16) is replaced by a narrow band $\epsilon_l^{(n)}(\mathbf{q},j)$ (always larger than the cutoff energy $\epsilon_{c-o}$), which is a function of the unperturbed phonon wave vector and branch. In other words, any phonon in the first Brillouin zone of bulk solid $D_2$, characterized by an energy $\hbar\omega(\mathbf{q},j)$, gives rise to a slightly different localized lattice vibration, provided with an energy $\epsilon_l^{(n)}(\mathbf{q},j)$. Implementing this approach to the conditions of sample 4, one can work out the localized lattice vibration band (ranging from 10.40 to 11.19 meV), and from this, a different version of $Z_{\mathrm{H}}^{(4)}(\epsilon)$, still reported in Fig. 8 after an appropriate broadening. It is easy to verify that the introduction of the method has changed the simulated $H_2$-defect DoPS in a very modest way, leaving the disagreement between theoretical and experimental data almost unchanged. Calculations using hydrogen concentration values as in samples 2 and 3 produced similar results.

Surely among the various deficiencies of the defect theories so far applied, the most relevant one appears to be the total lack (in the single impurity calculation) or the strong underestimation (in the finite concentration calculation) of the anharmonic damping of the $H_2$ localized modes. In practice, keeping in mind Eq. (11), one of the missing part of the calculations is the anharmonic one-phonon response function $A(\mathbf{q},j;\epsilon)$ for the $H_2$ defects, which, in a very coarse picture,[38] could be reduced in our case to a simple diagonal form: $A(\epsilon-\epsilon_l^{(n)})$. Some rough information on this hypothetical response function can be obtained operating a heuristic subtraction of the propagating part from the experimental $\tilde{Z}(\epsilon)$, and deconvoluting the localized part of the calculated $Z_{\mathrm{H}}^{(4)}(\epsilon)$ from the rest of the experimental data, properly taking into account the instrumental and intrinsic broadening of the latter. In the case of sample 4, the theoretical localized modes from the finite concentration theory need to undergo a shift of about 1 meV (unphysically to the right) and a broadening characterized by additional FWHM of 4.0–4.5 meV to optimize the comparison with the experimental data. However, these results cast some doubts on the suggested interpretation: the latter figure looks suspiciously large for an anharmonic damping [e.g., bulk solid hydrogen at $T=4$ K exhibits an equivalent damping of 0.95 meV at $\epsilon\simeq 10$ meV (Refs. 38 and 41)] and, moreover, anharmonic renormalization should lower phonon energies instead of increasing them. So these remarks, together with the number of visible peaks in the experimental data, suggest a different and more complex interpretation of the structured phonon spectra of hydrogen defects in solid deuterium, in which the existence of some localized lattice vibrations placed in broad energy interval, namely, 7–17 meV, plays a more important role than the simple anharmonic damping itself. For example, if the presence of two main peaks placed 5 meV apart is assumed, then since the ratio between their areas is roughly 2:1, one could conjecturally attribute the higher energy peak to the lattice vibrations along the **c** axis of the hcp crystal (around 15 meV), and the lower energy peak to those perpendicular to it (around 10 meV). However, as mentioned above, some caution is needed dealing with the spectral features between 14 and 16 meV, which appear to vary with the hydrogen concentration (see Fig. 7) and might have a completely different origin. For example, a small ortho-hydrogen contamination present in the mixture in place of p-$H_2$ could give rise to a peak corresponding to the $J=1\rightarrow J'=2$ transition (with $E_{1-2}=29.2$ meV), which, after subtracting $E_{0-1}$, would appear exactly in the spectral zone we are considering. For this reason we are not going to speculate any longer on the number of peaks present in the 7–17 meV interval of the experimental $\tilde{Z}(\epsilon)$.

The last comparison to be established concerns our experimental data and the results of the combined use of self-consistent phonon approximation and coherent potential ap-

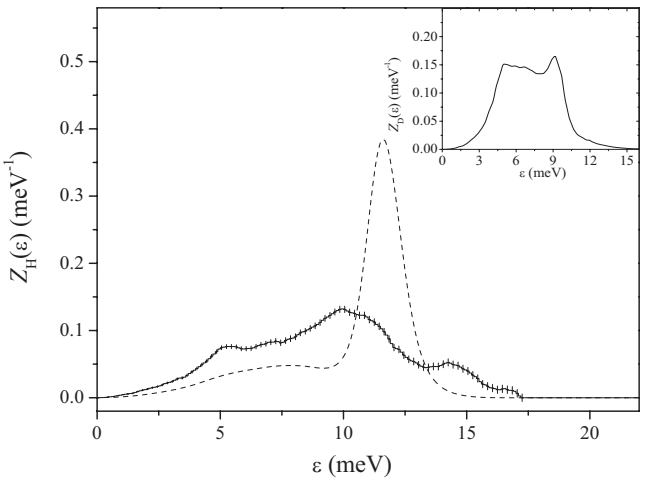


FIG. 9. Experimental (full line plus error bars) and self-consistent phonon approximation estimate (dashed line) of the hydrogen-defect density of phonon states in a solid deuterium matrix (Ref. 53) for sample 4. The inset (upper right corner) reports the pure solid ortho-deuterium ($T=0$, $n=30.16$ nm$^{-3}$) density of phonon states derived from Ref. 53.

proximation, as implemented in Refs. 17 and 53. In the latter of these studies, lattice dynamics calculations on pure ortho-deuterium and on its mixture with 1% of para-hydrogen, both at $T=0$ and assuming hcp lattices, have been performed. The calculated density of phonon states for o-$D_2$ (see inset in Fig. 9) is characterized by a lattice constant $a=3.606$ Å and a mean squared displacement of the molecular center of mass $\langle \mathbf{u}^2 \rangle = 0.25$ Å$^2$, which compare well with the literature data, respectively, in Refs. 20 and 54.

However, as for the detailed spectral features, we have to observe that noticeable differences between the pure deuterium DoPS's in the insets of Figs. 8 and 9 do exist. Dealing with para-hydrogen defects in ortho-deuterium matrices, the lattice dynamical calculation by Menn[53] provides the following values for the average lattice constant and the mean squared displacement of the $H_2$ center of mass: $a=3.592(2)$ Å (i.e., $n=30.51$ nm$^{-3}$) and $\langle \mathbf{u}^2 \rangle = 0.325(1)$ Å$^2$, respectively. It is important to note that the present $\langle \mathbf{u}^2 \rangle$ value might seem largely dissimilar from those in Table II, but some of this discrepancy is just due to the different values of temperature and density considered. Thus, after a slight rescaling through the average deuterium Grüneisen parameter[50] [$\gamma=1.88$ (Ref. 38)] to match the experimental density of sample 4, the calculated p-$H_2$-defect DoPS exhibits a $\langle \mathbf{u}^2 \rangle = 0.351(1)$ Å$^2$ if evaluated at $T=13.68$ K. Similarly, one obtains $\langle E_k \rangle = 90.8(3)$ K. Both these figures, although not far from the experimental and PIMC values in Table II, are already the mark of some imperfection. After including appropriate instrumental and rotational broadening effects, the calculated (and corrected through the average Grüneisen parameter[50]) DoPS is finally reported in Fig. 9. The agreement with the experimental data (e.g., from sample 4) is still unsatisfactory, since this calculated DoPS appears qualitatively rather similar to the two harmonic evaluations plotted in Fig. 8. However, some differences among the three simulated DoPS's are indeed visible: the self-consistent phonon estimate shows a localized mode peak broader than the harmonic ones, in this respect a little closer to the experimental data, but, on the contrary, the peak position is better reproduced in the harmonic cases. A similar conclusion can be drawn for the propagating part of $Z_H^{(4)}(\epsilon)$ (say, for $\epsilon < 10$ meV), where the self-consistent phonon estimate is less precise. In any case, the problem envisaged after the comparison between experimental data and harmonic calculations (namely, the excess in the spectral width) is still present and unsolved even after taking into account the self-consistent phonon simulation.

Before ending this section, it is worthwhile to mention a hypothetical alternative cause of the anomalous broadening of the impurity spectrum $\tilde{Z}(\epsilon)$. One might think that the presence of a large number of imperfections in the $D_2$ lattice doped with $H_2$, such as empty crystal sites adjacent to an $H_2$ impurity, could give rise to a band blurring which spectroscopically could be confused with a large phonon damping. Giving the lack of the present samples' diffraction patterns, we have to address this hypothesis indirectly. We think that it is implausible for the following reasons.

(i) The spectral broadening appears to be largely $H_2$-concentration independent, so the hypothetical sample imperfections should be related to the $D_2$ polycrystals themselves, not to the fact that we are dealing with a quantum alloy. However, in the literature on solid deuterium, the general notion is quite the opposite: samples grown from a slow cooling of the liquid at low pressure are reported to be good quality and strain free polycrystals.[55]

(ii) Lattice imperfections should give rise to a spectral broadening exhibiting similar values in the elastic line region and in the defect density of phonon states, but, as seen above, this is not the case.

(iii) As we have noted above looking in Fig. 8, one can see that the first part of the defect density of phonon states (i.e., the propagating part) is reasonably well described by the Eq. (16), making use of the solid deuterium density of phonon states from Ref. 38 (inset in Fig. 8). On the contrary, the second part (i.e., the localized part) looks extremely broader than the predictions of Eq. (16). Once again, lattice imperfections should give rise to a spectral broadening, exhibiting similar values in the propagating region of the defect density of phonon states and in the localized one. However, as seen in Fig. 8, this is not the experimental result.

## V. CONCLUSIONS

In the present study, we have measured incoherent inelastic neutron scattering from para-hydrogen defects in solid normal deuterium matrices at three different concentration levels (between 3% and 11%) using the time-of-flight neutron spectrometer TOSCA-II. The measured double-differential cross sections have provided experimental access (through an elaborated data analysis) to the self-part of the inelastic structure factor for the centers of mass of the $H_2$ defects in the samples under observation. The measured data were corrected for the typical experimental effects, subtracted of the deuterium signal, and then analyzed in the

framework of the modified Young-Koppel model to remove the contributions coming from the rotational dynamics. On the other hand, the Gaussian approximation has been assumed for the low-energy spectral range, aiming to relate the incoherent scattering law of the para-hydrogen defects to their densities of phonon states. These spectral functions have been subsequently obtained through an accurate self-consistent procedure able to evaluate (and then remove) the undesired multiphonon contributions. The final densities of phonon states came out to be broad, structured, and essentially concentration independent. In addition, two Bose-corrected moments of these spectral functions were related to important physical quantities concerning the molecular center-of-mass dynamics (namely, mean squared displacement and mean kinetic energy). The former was compared to an independent experimental estimate from the sharp rotational line placed at $E=14.5$ meV, while the latter was simulated through a path integral Monte Carlo code.

The results of these two comparisons turned out to be very satisfactory, providing a strong validation of our detailed data analysis, that, despite its complexity, produced reliable densities of phonon states for the para-hydrogen defects. Subsequently, processed experimental data were compared to some calculations, gradually more and more advanced, starting from a simple harmonic model at infinite dilution, then including concentration effects (always in a harmonic framework), and finally moving to a fully independent lattice dynamics simulation,[53] based on the joint use of self-consistent phonon approximation and coherent potential approximation. However, while the description of the first part of the defect density of phonon states, attributed to the modes propagating in lattice, turned out to be reasonably acceptable for the first two calculations, the localized part of the spectrum was properly described by none of them. The position of the mean frequency value was approximately well reproduced by all the three models, but as far as the large overall width (about 4 meV/$\hbar$) is concerned, experimental data appear at this stage impossible to be fully explained. A tentative description of this finding could explain it as an extremely severe localized-mode damping. Thus, our final results can be said to represent a sort of challenge for theoreticians and computational physicists involved in the important task of implementing and improving quantum dynamic simulation techniques. In this respect, we have to mention a very preliminary ring polymer molecular dynamics calculation dealing with a system similar to sample 4, namely, composed of 180 deuterium molecules plus 18 hydrogen ones.[56] Despite the simulation work is still in progress, it seems that the capability of this technique to reproduce the main features of the experimental phonon spectrum is much greater than that of the calculations reported in Figs. 8 and 9. In addition, on the experimental side, it would be very interesting to assess the action of the $J=1$ fraction of $D_2$ molecules on the p-$H_2$ defect dynamics, repeating the present experimental work with an ortho-deuterium matrix replacing the normal deuterium one.

## ACKNOWLEDGMENTS

This work has been financially supported by C.N.R. (Italy) and, in part, by Ente Cassa di Risparmio di Firenze (Project Firenze-Hydrolab). The Cooperation Agreement No. 01/9001 between CNR and CCLRC, concerning collaboration in scientific research at the spallation neutron source ISIS (UK), is gratefully acknowledged. The authors acknowledge the skillful technical help from the ISIS User Support Group.

[1] N. R. Werthamer, Am. J. Phys. **37**, 763 (1969).
[2] T. Markovich, E. Polturak, J. Bossy, and E. Farhi, Phys. Rev. Lett. **88**, 195301 (2002).
[3] M. A. Lee, K. E. Schmidt, M. H. Kalos, and G. V. Chester, Phys. Rev. Lett. **46**, 728 (1981).
[4] W. M. C. Foulkes, L. Mitas, R. J. Needs, and G. Rajagopal, Rev. Mod. Phys. **73**, 33 (2001).
[5] D. M. Ceperley, Rev. Mod. Phys. **67**, 279 (1995).
[6] H. R. Glyde, *Excitations in Solid and Liquid Helium* (Oxford University Press, Oxford, 1994).
[7] R. Senesi, C. Andreani, D. Colognesi, A. Cunsolo, and M. Nardone, Phys. Rev. Lett. **86**, 4584 (2001).
[8] G. Voth, Adv. Chem. Phys. **93**, 135 (1996).
[9] I. R. Craig and D. E. Manolopoulos, J. Chem. Phys. **122**, 084106 (2005).
[10] D. Colognesi, M. Celli, and M. Zoppi, J. Chem. Phys. **120**, 5657 (2004).
[11] H. Saito, H. Nagao, K. Nishikawa, and K. Kinugawa, J. Chem. Phys. **119**, 953 (2003).
[12] R. J. Elliot, J. A. Krumhansl, and P. L. Leath, Rev. Mod. Phys. **46**, 465 (1974).
[13] B. M. Powell and M. Nielsen, Phys. Rev. B **12**, 5959 (1975).
[14] B. A. Fraass and R. O. Simmons, Phys. Rev. B **36**, 97 (1987), and references therein.
[15] I. F. Silvera and V. V. Goldman, J. Chem. Phys. **69**, 4209 (1978).
[16] C. M. Varma, Phys. Rev. A **4**, 313 (1971); R. D. Nelson and W. H. Hartmann, Phys. Rev. Lett. **28**, 1261 (1972).
[17] K. Menn and W. Biem, J. Low Temp. Phys. **57**, 1 (1984).
[18] J. E. Gubernatis and J. A. Krumhansl, J. Appl. Phys. **46**, 1875 (1975).
[19] D. Colognesi, M. Celli, F. Cilloco, R. J. Newport, S. F. Parker, V. Rossi-Albertini, F. Sacchetti, J. Tomkinson, and M. Zoppi, Appl. Phys. A: Mater. Sci. Process. **74**, 64 (2002).
[20] *Physics of Cryocrystals*, edited by V. G. Manzhelii and Yu. A. Freiman (American Institute of Physics, Woodbury, NY, 1996).
[21] J. van Straaten and I. F. Silvera, Phys. Rev. B **37**, 1989 (1988).
[22] G. N. Shcherbakov, Sov. J. Low Temp. Phys. **17**, 73 (1991).
[23] M. Nielsen, Phys. Rev. B **7**, 1626 (1973).
[24] S. N. Ishmaev, I. P. Sadikov, A. A. Chernyshov, G. V. Kobelev, V. A. Sukhoparov, and A. S. Telepnev, Sov. Phys. JETP **75**, 382 (1992).
[25] R. D. McCarty, J. Hord, and H. M. Roder, *Selected Properties of Hydrogen*, NBS Monograph Vol. 168 (U.S. Department of Commerce, Washington, D.C., 1981).

[26] I. F. Silvera, Rev. Mod. Phys. **52**, 393 (1980).
[27] R. Treviño Arizpe, Rev. Mex. Fis. **4**, 23 (1955).
[28] R. A. Cowley, J. Phys.: Condens. Matter **15**, 4143 (2003).
[29] A. K. Agrawal, Phys. Rev. A **4**, 1560 (1971); V. F. Sears, Adv. Phys. **24**, 1 (1975).
[30] W.-D. Seiffert, Report No. EUR 4455d, 1970 (unpublished); W.-D. Seiffert, B. Weckermann, and R. Misenta, Z. Naturforsch. A **25A**, 967 (1970).
[31] S. W. Lovesey, *Theory of Neutron Scattering from Condensed Matter* (Oxford University Press, Oxford, 1987), Vol. I.
[32] D. Colognesi, M. Celli, M. Neumann, and M. Zoppi, Phys. Rev. E **70**, 061202 (2004).
[33] M. Zoppi, Physica B **183**, 235 (1993).
[34] J. A. Young and J. U. Koppel, Phys. Rev. **135**, A603 (1964).
[35] V. F. Turchin, *Slow Neutrons* (Israel Program for Scientific Translation, Jerusalem, 1965), p. 108.
[36] A. Rahman, K. S. Singwi, and A. Sjölander, Phys. Rev. **126**, 986 (1962).
[37] D. Colognesi, C. Andreani, and E. Degiorgi, J. Neutron Res. **11**, 123 (2003).
[38] J. W. Schmidt, M. Nielsen, and W. B. Daniels, Phys. Rev. B **30**, 6308 (1984).
[39] H. Horner, Phys. Rev. Lett. **29**, 556 (1972).
[40] H. R. Glyde, J. Low Temp. Phys. **59**, 561 (1985).
[41] A. Bickermann, H. Spitzer, H. Stiller, H. Meyer, R. E. Lechner, and F. Volino, Z. Phys. B **31**, 345 (1978).
[42] H. R. Glyde and S. I. Hernadi, Phys. Rev. B **25**, 4787 (1982).
[43] B. Fåk and B. Dorner, Institut Laue-Langevin Technical Report No. 92FA008S, 1992 (unpublished).
[44] A. I. Kolesnikov and J.-C. Li, Physica B **234-236**, 34 (1997); J. Dawidowski, F. J. Bermejo, and J. R. Granada, Phys. Rev. B **58**, 706 (1998).
[45] A. B. Harris, Phys. Rev. B **1**, 1881 (1970).
[46] R. J. Elliott and W. M. Hartmann, Proc. Phys. Soc. London **90**, 671 (1967).
[47] M. J. Norman, R. O. Watts, and U. J. Buck, J. Chem. Phys. **81**, 3500 (1984).
[48] M. Neumann and M. Zoppi, Phys. Rev. A **40**, 4572 (1989).
[49] M. Zoppi and M. Neumann, Phys. Rev. B **43**, 10242 (1991).
[50] E. R. Cowley and R. A. Cowley, Proc. R. Soc. London, Ser. A **287**, 259 (1965).
[51] G. F. Nardelli and N. Tettamanzi, Phys. Rev. **126**, 1283 (1962); R. D. Williams and S. W. Lovesey, Z. Phys. B: Condens. Matter **62**, 413 (1986).
[52] D. W. Taylor, Phys. Rev. **156**, 1017 (1967).
[53] K. Menn, Ph.D. thesis, Justus Liebig University, 1983.
[54] I. F. Silvera, W. N. Hardy, and J. P. McTague, Phys. Rev. B **5**, 1578 (1972).
[55] P. E. Sokol, R. O. Simmons, J. D. Jorgensen, and J. E. Jørgensen, Phys. Rev. B **31**, 620 (1985).
[56] D. E. Manolopoulos and S. Habershon (private communication).